Potential of SAR-derived features for detecting structural variations in coffee plots

João Pedro Marochio Correa [1], Maria de Lourdes Bueno Trindade Galo [1], Gleice Aparecida de Assis [2], Nelson Lemes Neto [1]

[1] São Paulo State University (UNESP), Presidente Prudente, São Paulo, Brazil - joao.marochio-correa@unesp.br, nelson.lemes@unesp.br, trindade.galo@unesp.br
[2] Federal University of Uberlândia (UFU), Monte Carmelo, Minas Gerais, Brazil - gleice@ufu.br

Keywords: Remote Sensing, Synthetic Aperture Radar, Backscatter Coefficient, Coffee Cultivation, Precision Agriculture.

Abstract

Brazil is the world's top producer and exporter of coffee, making it a key player in the global supply chain. This study investigates the potential of C-band Synthetic Aperture Radar (C-SAR) imagery from Sentinel-1 to detect structural differences in coffee plantations with varying cultivars and planting ages. A two-year time series of monthly radar images from Sentinel-1B and optical images from Multispectral Instrument (MSI) abord Sentinel-2 were used to compare radar-derived polarimetric features with the optical Normalized Difference Vegetation Index (NDVI). The research was conducted at Fazenda Juliana, a commercial coffee farm in Minas Gerais, which provided detailed plot boundaries and planting records. SAR data were processed using the Sentinel Application Platform (SNAP) to generate backscatter coefficients (σ^0) in VH and VV polarizations. Four polarimetric indices, Cross Ratio (CR), Normalization Ratio (NL), Radar Gap Index (RGI), and Radar Vegetation Index (RVI) were calculated. These SAR features and NDVI values were segmented by plot boundaries, and average values were extracted for each plot. The temporal analysis revealed a slight cyclical trend in both radar backscatter and NDVI across the plots. A consistent positive correlation was observed between σ^0_{VV} and NDVI, especially in plots with atypical vegetation responses. On specific date, NDVI fluctuations showed a strong correlation ($r > 0.9$) with σ^0 and NL, indicating their potential to capture structural variation in coffee crops. These results also demonstrate that radar-based features, particularly when optical data is limited, offer a reliable method for monitoring crop variability and plantation structure.

1. Introduction

Brazil stands as the world's leading coffee producer and exporter, playing a crucial role in global supply. For the 2024-2025 harvest, the country is expected to yield approximately 51.81 million bags of coffee. This volume accounts for 29.62% of global coffee production, reinforcing Brazil's dominance in the industry (Ferreira & Cavaton, 2025). In coffee production, the biennial effect is a phenomenon marked by alternating cycles of large and small harvests over time (Mendonça et al., 2011). This effect is explained by the competition between the plant's vegetative and reproductive functions. During high-yield years, the plant directs its energy toward fruit growth, limiting vegetative development. Since the fruit of the coffee tree emerges on branches from the previous year, this leads to reduced production in the subsequent cycle, which spans approximately two years (Tolentino, 2023). Over time, various models have been developed to represent the phenological phases of the coffee tree, with classifications ranging from four to eight phases (Camargo, 1998).

Monitoring crops throughout their phenological cycle enables more efficient planning across the production chain and supports the development of models for estimating productivity. One of the key advantages of such prediction is its ability to provide better control over fluctuations in sales prices, while also optimizing the use of storage resources, operational efficiency, logistics, and marketing strategies (Jin et al., 2018; Delécolle et al., 1992).

Remote Sensing (RS) is one of the most effective automated data collection technologies for surveying and monitoring land resources at global, regional, and local scales. By analyzing the interaction of electromagnetic energy with targets on Earth's surface (Figueiredo, 2005; Meneses & Almeida, 2012), RS enables the monitoring of crop development, the identification of potential issues, and the prediction of agricultural productivity (Fountas et al., 2020). The widespread adoption of optical RS has enabled the extraction of extensive information on agricultural crops through spectral bands available in satellite imagery captured by optical sensors, such as the Landsat and Sentinel-2 series. Various agronomic applications leverage optical RS, particularly spectral indices, to predict crop yield and biomass, monitor plant vigor and water stress, and analyze phenological stages (Brandão, 2009). Among these indices, the Normalized Difference Vegetation Index (NDVI) is the most widely used in optical RS. It serves cover and for assessing biomass levels, evaluating crop health and yield, estimating vegetation cover, and supporting a range of other agricultural applications (Abreu & Coutinho, 2014; Paruelo et al., 2000).

Crop analysis approaches based on their temporal behavior demonstrate greater accuracy and robustness compared to traditional methods that rely on the processing of individual images (Jönsson et al., 2018). In particular, the use of time series of vegetation indices allows the monitoring of phenology and intra-seasonal variations in areas designated for agricultural activity (Arvor et al., 2011). However, obtaining regular time series of optical data for the efficient monitoring of large areas is limited by the scarcity of data that combine high spatial and temporal resolution, in addition to the atmospheric effects.

Synthetic Aperture Radar (SAR) sensors operate within the microwave range of the electromagnetic spectrum, which is largely unaffected by atmospheric conditions. This enables the acquisition of agricultural data even under cloud cover (Moran et al., 1998). While optical sensors are sensitive to vegetation characteristics related to photosynthetic activity and biomass, SAR sensors detect microwave energy reflected from internal canopy structures, including leaves, branches, and stems. This capability allows for detailed assessments of vegetation geometry and moisture content (Ulaby et al., 1984). Moreover, SAR backscatter intensity responds to changes in vegetation structure, making it a powerful tool for monitoring growth and phenological shifts (Li et al., 2023).

This contribution has been peer-reviewed. The double-blind peer-review was conducted on the basis of the full paper.
https://doi.org/10.5194/isprs-annals-X-3-W4-2025-85-2026 | © Author(s) 2026. CC BY 4.0 License.

The Sentinel missions, developed by the European Space Agency (ESA) as part of the Copernicus program, comprise a series of satellite systems designed for comprehensive Earth observation and environmental monitoring. Sentinel-1 is equipped with SAR instruments, operating in the C-band with dual polarization, utilizing VV and VH modes and Sentinel-2, an optical system, provides a 5-day revisit cycle and features 13 spectral bands.

Given the importance of temporal data in ensuring consistent observations, this study investigates the potential of C-SAR Sentinel-1 imagery for detecting structural variations in coffee plantations across different cultivars and age groups. The analysis explores the relationship between SAR backscattered signals in VV and VH polarizations and optical NDVI values, based on a two-year series of monthly images. Additionally, it compares these radar signals and NDVI values to polarimetric indices derived from a single SAR acquisition on October 6, 2021.

2. Methodology

2.1 Study Area

The study was was carried out in a commercial experimental area located at Fazenda Juliana in the municipality of Monte Carmelo, state of Minas Gerais, within the Triângulo Mineiro and Alto Paranaíba Mesoregion. The site is centered at Latitude: 18°42'29.85" S and Longitude: 47°32'49.67" W, with an average altitude of 880 m and a gently undulating terrain. The local climate is classified as tropical with a dry season (Aw), according to the Köppen–Geiger system. Figure 1 provides an overview of the study area, highlighting the coffee plots of *Coffea arabica L* examined in this research. These plots are delineated using a color composition derived from a Sentinel-2B optical image acquired on October 6, 2021.

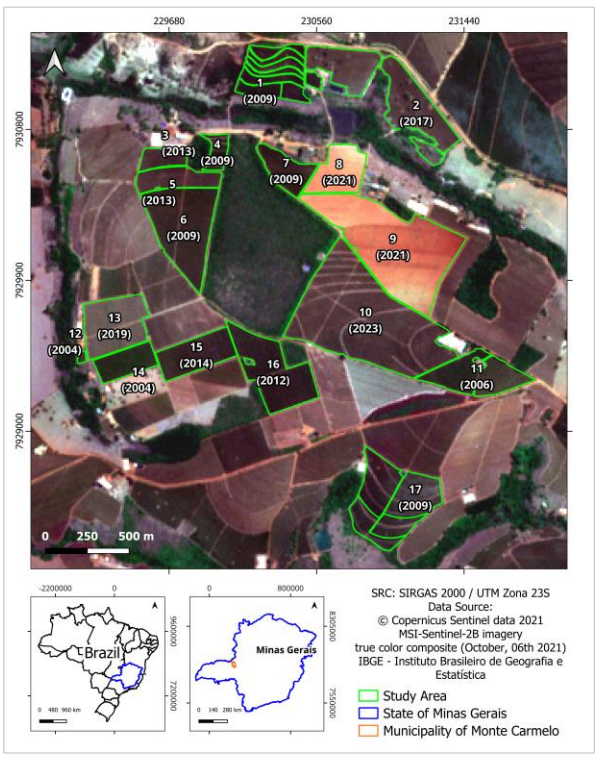

Figure 1 - Location map of the study area showing the coffee plots outlined in green over a true-color Sentinel-2B image. The composition uses the Red (664.9 nm), Green (558.9 nm), and Blue (492.3 nm) spectral bands.

The delimitation of the 17 coffee production plots analyzed in this study (Figure 1), along with detailed information regarding planting age and cultivars (Table 1), was provided directly by Fazenda Juliana.

n°	Plot name	Cultivar	Year	Area (ha)
1	Fava 2	Topázio MG-1190	2009	11.54
2	Fava 3	Mundo Novo	2017	20.5
3	Creoulo Novo ST 1	Mundo Novo	2013	2.97
4	Creoulo Setor 11	Bourbon amarelo e Obatã IAC 1669-20	2009	2.6
5	Creoulo Novo ST 2-3	Bourbon amarelo	2013	5.84
6	Creoulo Velho St 4-10	Mundo Novo	2009	17.29
7	Soldado	Mundo Novo	2009	5.54
8	Fava 1 ST 1	Catuaí Vermelho IAC 99	2021	7.49
9	Fava 1 ST 2-5	Paraiso	2021	32.08
10	Sede Paraiso	Paraiso	2023	41.52
11	Sede Novo (Obatã)	Obatã IAC 1669-20	2006	10.5
12	Paraiso	Paraíso MG H 419-1	2004	0.35
13	NSA 1	Catuaí Vermelho IAC 144	1999	11.03
14	IAPAR 59	Iapar 59	2004	5.54
15	NSA 2	Mundo Novo	2014	8.52
16	Baltazar	Mundo Novo	2012	15
17	Gui	Catuaí Vermelho IAC 99	2009	18.5

Table 1 – Overview of coffee plots within the study area, detailing plot name, cultivar, planting year, and planted area (in hectares). (Adapted from Fazenda Juliana).

2.2 Characterization of the coffee crop

The coffee plant is a perennial shrub characterized by a complex phenological cycle, which consists of a succession of vegetative and reproductive phases spanning approximately two years. The first year is dedicated to vegetative growth, focusing on branch and foliage development. In the second year, resources shift towards flowering and fruit formation, resulting in alternating periods of high and low productivity, known as the biennial effect. This cycle can be further subdivided into distinct phenological stages, as illustrated in Figure 2.

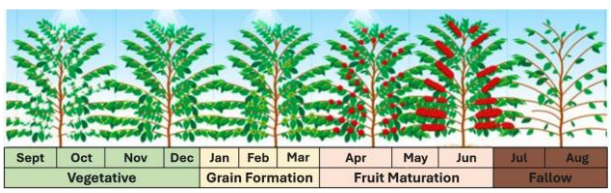

Figure 2 - Phenological cycle of coffee cultivation. (Source: Adapted from Camargo, 1998).

According to Camargo (1998), the phenological cycle of *Coffea arabica L* for the tropical conditions of Brazil can be subdivided into four different phases:

- 1st Phase – It takes place from September to December, characterized by long days (13 - 14 hours of effective light) where vegetative development takes place.

• 2nd Phase – The second phenological phase generally occurs from January to March, characterized by short days (less than 13 hours of light). The flower buds mature after accumulating around 350 mm of potential evapotranspiration (ETp) and go into dormancy, awaiting anthesis (flowering). In the last two months, the dormant buds generate small leaves, characterizing the separation of the first from the second phenological year.

• 3rd Phase – From April to June, fruit maturation depends on the periodicity of the cultivar and the accumulated solar energy (~700 mm of ETp). Moderate water deficits can benefit fruit quality.

• 4th Phase – The fourth phase takes place from July to August and is characterized by the coffee tree's autopod and the drying and death of many tertiary and quaternary branches.

The diagram shown in Figure 2 is repeated every year; however, the phenological cycle of the coffee tree is completed in two years, covering the vegetative period and the reproductive period. After a very productive crop, the plant needs time to recover, which leads to a less productive crop the following year.

2.3 Materials

The Sentinel datasets were obtained from the official repository, i.e., the European Space Agency (ESA) Copernicus Open Access Hub portal, available at https://scihub.copernicus.eu/ (exploiting the free, full and open Copernicus license). Monthly images from the Sentinel-1B and Sentinel-2 (A and B) systems were selected from January 2020 to December 2021.

Optical imagery from the Multispectral Imager (MSI) onboard the Sentinel-2A and Sentinel-2B satellites was selected based on cloud-free conditions over the study area. Consequently, no usable data were available for April, May, November, and December 2020, as well as February 2021. A total of 17 cloud-free scenes were acquired at Level-2A, which provides atmospherically corrected surface reflectance products.

The Sentinel-2 provides a 5-day revisit cycle and features 13 spectral bands, encompassing visible, near-infrared (NIR), and shortwave-infrared (SWIR) spectra, with a spectral coverage from 442.3 to 2185.7 nm. These bands are available at three distinct spatial resolutions (10, 20, and 60 meters) (ESA, 2024). For vegetation analysis, the red and near-infrared bands were employed to calculate the NDVI, achieving a spatial resolution of 10 meters.

Additionally, SAR images were acquired in the same time window, in Interferometric Wide Swath (IW) mode, utilizing Vertical-Horizontal (VH) and Vertical-Vertical (VV) polarizations. The 24 monthly images were processed at Ground Range Detected (GRD) level 1, achieving a spatial resolution of 10 meters. A GRD image is a product that has already been intensity detected, projected onto the ground, and is ready for analysis in various applications (ESA, 2024).

In the SAR analysis it is important to highlight the image formation process. The amount of energy scattered back to the radar sensor after interacting with vegetation structure components is proportional to the characteristics of the transmitted energy-specifically, its frequency and polarization. The signal's interaction is influenced by whether it undergoes polarization (horizontal or vertical) upon encountering canopy elements, the extent of its penetration into the vegetation, and its potential interaction with the ground surface. The degree of penetration into the plant canopy is primarily determined by the wavelength of the microwave radiation (Jensen, 2009). Figure 3 illustrates a comparison of how active microwave energy responds to different wavelengths in the L, C, and X bands within a hypothetical pine forest.

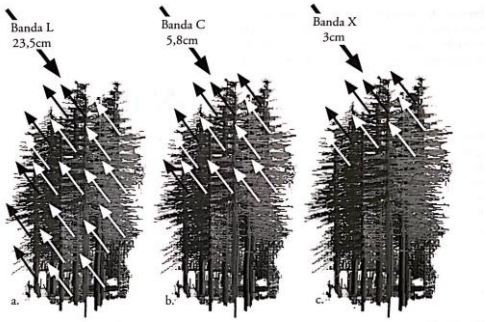

Figure 3 - Typical behavior of the active microwave signal, for different bands (L, C and X) with different wavelengths, in a hypothetical pine forest (Jensen, 2009).

The SAR Sentinel-1 image is acquired in the C band (5.8 cm), where the energy undergoes surface scattering at the top of the canopy and some volumetric scattering within the core of the stand. This interaction occurs as the energy interacts with leaves and branches, with some of it potentially reflecting off the ground surface. Additionally, a portion of the energy undergoes volumetric scattering, where it is scattered multiple times within a diffuse volume inside the trees, which may lead to depolarization.

Therefore, the utilization of C-band volumetric scattering and dual polarization is fundamental to the structural analysis of vegetation. A rigorous interpretation of Synthetic Aperture Radar (SAR) data is required to determine the volumetric backscatter, which corresponds to the proportion of microwave energy reflected by the vegetation canopy. This parameter is quantified by the backscatter coefficient, commonly referred to as sigma nought (σ^0).

2.4 SAR image pre-processing

The Sentinel-1B SAR image was initially pre-processed using the Sentinel Application Platform (SNAP) software, following the SAR data processing chain to achieve the Ground Range Detected (GRD) processing level (Figure 4).

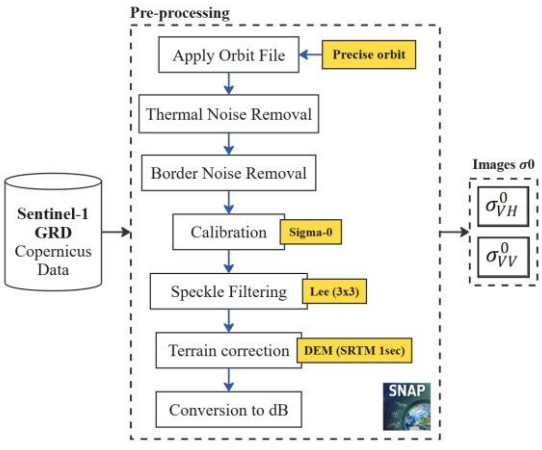

Figure 4 - Sentinel-1B GRD pre-processing workflow. Adapted from ESA (2024) and Tolentino (2023).

The initial pre-processing step, the Apply-Orbit-File, corrects the satellite's orbit using Sentinel-1 orbit data. Precise orbit files, automatically retrieved from the ESA GNSS Hub, were applied using a third-degree polynomial, following the standard procedure.

Thermal noise was corrected using a product-provided Look-Up Table and bilinear interpolation, while edge noise from raw data processing was addressed with default Border Noise Removal settings (ESA, 2024).

The radiometric calibration was conducted to compute sigma-0 (σ^0) backscattering coefficients for VH and VV polarizations, as described by Equation 1.

$$\sigma_i^0 = \frac{|ND_i|^2}{A_i^2}, \quad (1)$$

σ_i^0 represents the backscatter values per unit area in the terrain range, ND denotes the original digital number, and A_i is the calibration coefficient extracted from calibration Look-Up Tables (LUTs).

Speckle noise in SAR imagery may be mitigated through spatial or multilook filtering methods (ESA, 2024). In this analysis, the Lee filter was applied, which operates under the assumption of a local Gaussian distribution of pixel intensities to reduce noise while retaining image features (Lee, 1983). A 3 × 3 pixels window was utilized to preserve textural information and minimize the extent of smoothing.

Terrain correction in SAR imagery was performed using the Range Doppler Terrain Correction algorithm, which orthorectifies data based on orbital information, sensor parameters, and a Digital Elevation Model (DEM) (ESA, 2024). For this study, the SRTM (Shuttle Radar Topography Mission) 1Sec DEM was automatically retrieved via SNAP and applied with default settings, including nearest neighbor interpolation. Given the area's smooth topography, this approach was suitable. The correction followed Lee-filter-based speckle reduction in VH and VV polarizations. Backscattering coefficients (σ^0) images were extracted in the VH and VV polarizations, each with a spatial resolution of 10 meters, and subsequently converted into decibel (dB) units.

2.5 Derivation of Polarimetric Indices and Optical NDVI

The SAR image captured on October 19, 2021, was used to calculate the polarimetric indices (Table 2), which were compared with the optical NDVI, generated form a scene acquired on October 06, 2021.

Table 2 presents the set of polarimetric indices derived from the backscatter coefficients VH and VV of the SAR image and the respective operations involved in calculating these attributes. It also shows the formulation of the optical index NDVI.

The optical NDVI vegetation index (Table 2, gray-shaded line) was computed using surface reflectance values recorded in the Sentinel-2B Red band (Band 4, central wavelength: 664.9 nm) and Near-Infrared (NIR) band (Band 8A, central wavelength: 832.9 nm).

Index	Description	Equation	Reference
CR	*Cross Ratio*	$\frac{\sigma_{VH}^0}{\sigma_{VV}^0}$	(PALOSCIA *et al.*, 1999)
NL	*Normalization Ratio*	$\frac{\sigma_{VV}^0 * \sigma_{VH}^0}{\sigma_{VV}^0 + \sigma_{VH}^0}$	(LU *et al.*, 2011)
RGI	*Radar Gap Index*	$\frac{\sigma_{VV}^0 - \sigma_{VH}^0}{\sigma_{VV}^0 + \sigma_{VH}^0}$	(CASSOL *et al.*, 2019)
RVI	*Radar Vegetation Index*	$\frac{4 * \sigma_{VH}^0}{\sigma_{VV}^0 + \sigma_{VH}^0}$	(NASIRZADEHDIZAJI *et al.*, 2019)
NDVI	*Normalized Difference Vegetation Index*	$\frac{\rho NIR - \rho Red}{\rho NIR + \rho Red}$	(ROUSE *et al.*, 1973)

Table 2 – Polarimetric indices derived from C-SAR Sentinel-1B images, where σ_{VH}^0 and σ_{VV}^0 represent the backscattering coefficients in the VH and VV polarizations, respectively. The optical index was computed based on the surface reflectance (ρ) of the Sentinel-2B Near-Infrared (NIR) and the Red bands.

2.6 SAR features and optical NDVI comparisons

Monthly SAR backscatter coefficients in the VH and VV polarizations and NDVI images were utilized to monitor coffee cultivation plots. Pixel values corresponding to these features were extracted using 17 polygons that delineate representative coffee plots, as illustrated in Figure 1. This extraction process was conducted using Python.

Subsequently, the average values of the SAR attributes and the optical NDVI were computed for each polygon and organized into temporal sequences. For each of the 17 plots, time series of σ_{VH}^0 and σ_{VV}^0 were constructed using 24 monthly observations spanning from January 2020 to December 2021. In parallel, the NDVI time series was derived from 17 cloud-free optical satellite images obtained within the same time frame.

The temporal profiles of the NDVI and SAR-derived backscatter coefficients (σ_{VH}^0 and σ_{VV}^0) were visualized and examined through graphical representations and correlation analyses. These analyses aimed to explore the relationships between vegetation dynamics and radar signal responses across the monitored coffee plots.

Additionally, the average NDVI values obtained from the optical image dated October 6, 2021, were compared with the corresponding mean backscatter values derived from the SAR image acquired on October 19, 2021. This comparison also included polarimetric indices Cross Ratio (CR), Normalization Ratio (NL), Radar Gap Index (RGI), and Radar Vegetation Index (RVI) to further assess the sensitivity of radar metrics to vegetation conditions at the plot level.

Quantum Geographic Information System (QGIS) and Microsoft Excel were used to process raster data, compute statistical measurements for the plots, and analyze the correlation between optical NDVI and SAR features, among other tasks.

3. Results and discussion

3.1 Temporal Analysis of SAR Backscatter Coefficients and NDVI in Coffee Plantation

The time series of the average NDVI and SAR backscatter coefficients (σ^0_{VH} and σ^0_{VV}) of each one of the 17 evaluated plots, for the period from January 2020 to December 2021 are presented in Figure 5.

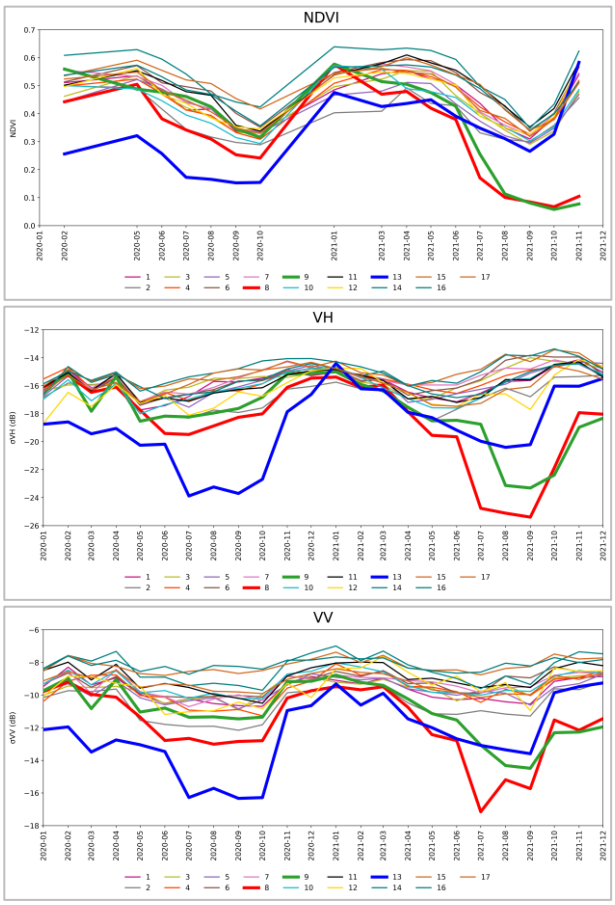

Figure 5 - Time series of the average monthly values of the NDVI, σ^0_{VH} and σ^0_{VV} features. Each of the 17 plotted lines corresponds to one of the coffee plots, numbered according to Figure 1 and Table 1.

The time series of average backscatter coefficients in VH and VV polarizations exhibit a subtle cyclical pattern, compared to the NDVI profiles. However, a temporal shift is observed in the minimum and maximum values across these datasets. Specifically, the lowest values of σ^0_{VH} and σ^0_{VV} were recorded between April and June, corresponding to the Fruit Maturation phenological phase. In contrast, the NDVI reached its minimum between August and October, aligning with the late Fallow period and the onset of the Vegetative phase. Despite this temporal displacement, the peak values of both NDVI and SAR backscatter coefficients tend to coincide with the transition from the end of the Vegetative phase to the beginning of Grain Formation. Although shifted by some months, the maximum values of NDVI and backscatter coefficients occur in the transition between the end of the Vegetative and the beginning of Grain Formation phases.

Since NDVI is an index derived from optical images it was not possible to obtain continuous data due to cloud cover in the study area. This effect does not occur in SAR images, which made it possible to generate continuous time series. The time series indicate that plots 8, 9, and 13 showed atypical responses compared to the others. Plots 8 and 9 were planted in 2021, which explains the lowest average σ^0 and NDVI responses observed in this period, probably due to the presence of exposed soil, recently prepared, harvested or fallow. Plot 13, on the other hand, being the oldest (Table 1), may have had a different response over the two years analyzed.

Figure 6 shows the correlations obtained from the comparison between the NDVI and the backscatter coefficient complete time series in VH and VV, for each of the 17 parcels with their respective planting years.

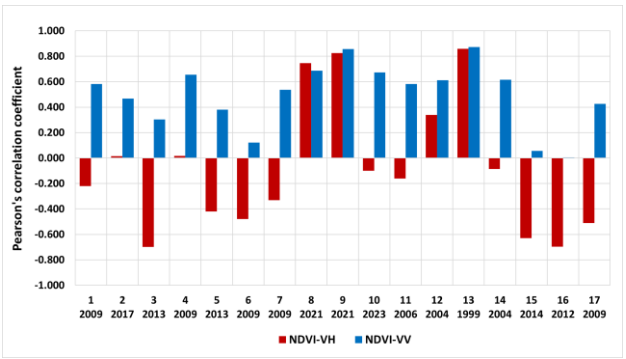

Figure 6 - Temporal Correlation between SAR backscatter coefficients and optical NDVI across coffee plots. Red bars indicate the correlation between σ^0_{VH}, and NDVI, while blue bars represent the correlation between σ^0_{VV} and NDVI for each of the 17 delineated coffee plots.

In the temporal analysis comparing NDVI with SAR backscatter coefficients in VV polarization, exclusively positive correlations were observed, ranging from negligible (plot 16, 0.0058) to strong (plot 13, 0.8730). Conversely, the majority of correlations between NDVI and VH-polarized backscatter were negative, with values spanning from –0.6993 (plot 3) to 0.8592 (plot 13). Notably, plots 8 and 9 exhibited atypical behavior compared to the general trend, recording high correlation values in both polarizations: 0.7453 and 0.8257 for NDVI and σ^0_{VH}, and 0.6874 and 0.8572 for NDVI and σ^0_{VV}. respectively. Similarly, plot 13 stood out by presenting the highest temporal correlations between NDVI and SAR backscatter coefficients in both VH and VV polarizations, underscoring its distinct structural response within the plantation.

3.2 Coffee plots analysis in SAR and optical images for a single data

Figure 7 shows spatial subsets of the 17 coffee plots, where grayscale shading represents the intensity values associated with NDVI and different SAR features. These include NDVI values from the optical image acquired on October 6, 2021; VH and VV backscatter coefficients from the SAR image dated October 19, 2021; and the polarimetric indices (CR, NL, RGI, and RVI) derived from the same SAR scene.

This contribution has been peer-reviewed. The double-blind peer-review was conducted on the basis of the full paper.
https://doi.org/10.5194/isprs-annals-X-3-W4-2025-85-2026 | © Author(s) 2026. CC BY 4.0 License.

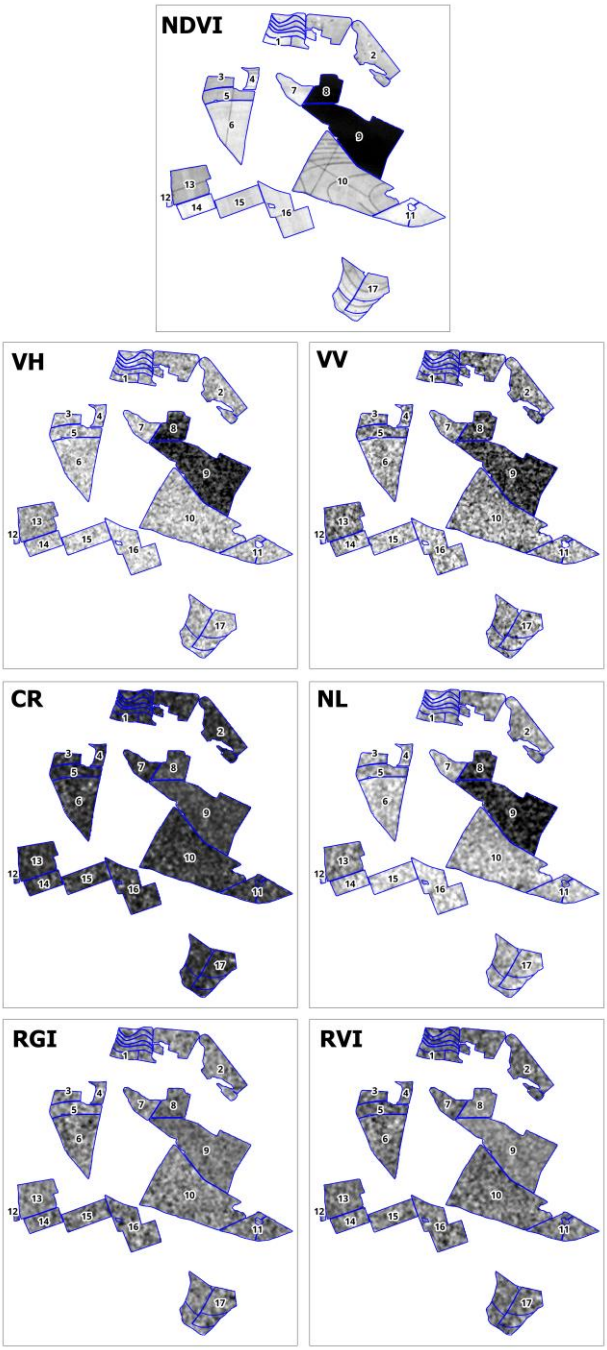

Figure 7 - Grayscale variability of NDVI, σ^0_{VH}, σ^0_{VV}, and the polarimetric indices CR, NL, RGI and RVI extracted from the 17 coffee plots cropped from the October 2021 images.

The NDVI and backscatter coefficients (σ^0_{VH} and σ^0_{VV}) showed similar behavior, characterized by low values (darker shades of gray) in plots 8 and 9 and higher values in the other plots. The polarimetric indices resulted in visually similar images, with similar values between plots, except in the case of the NL index, which showed reduced values and a downward trend associated with decreased vegetation cover.

Figure 8 graphically illustrates the interplot variability in NDVI and SAR backscatter coefficients (σ^0_{VH} and σ^0_{VV} in dB) across the 17 coffee plots, highlighting differences primarily associated with planting age.

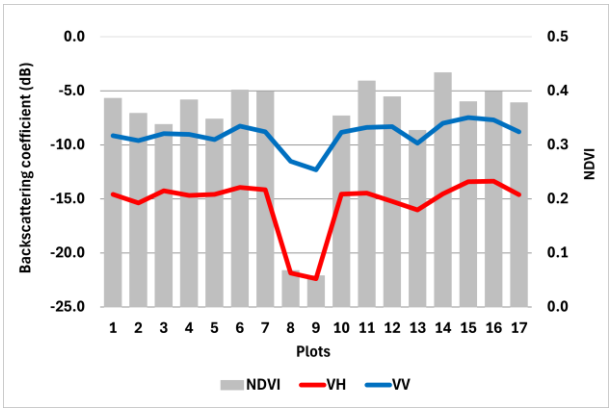

Figure 8 - Average σ^0_{VH} (red line) and σ^0_{VV} (blue line) in dB and the NDVI response (gray bars) for each of the 17 coffee plots.

It can be seen that the average σ^0_{VH} and σ^0_{VV} response of the plots follows a positive correlation in relation to the average NDVI response of the plots. Plots 8 and 9 stand out with the lowest average σ^0 and NDVI responses, being plots of exposed soil, recently prepared, harvested or fallow, which can be confirmed by looking at the color composition in Figure 1. The plots with the highest average NDVI response (e.g. plots 6, 7, 11, 14 and 16) indicate denser vegetation, as they are still in the Fruit Maturation stage or later management.

Subsequently, the relationships between the SAR backscatter coefficients (σ^0_{VH} and σ^0_{VV}) and the NDVI were quantified and visually represented (Figure 9). The correlation analysis revealed a strong linear association between σ^0_{VH} and NDVI, with a Pearson correlation coefficient (PCC) of 0.9642 and a coefficient of determination (R^2) of 0.9296. Similarly, the relationship between σ^0_{VV} and NDVI yielded a Pearson correlation coefficient of 0.9137 and an R^2 value of 0.8348.

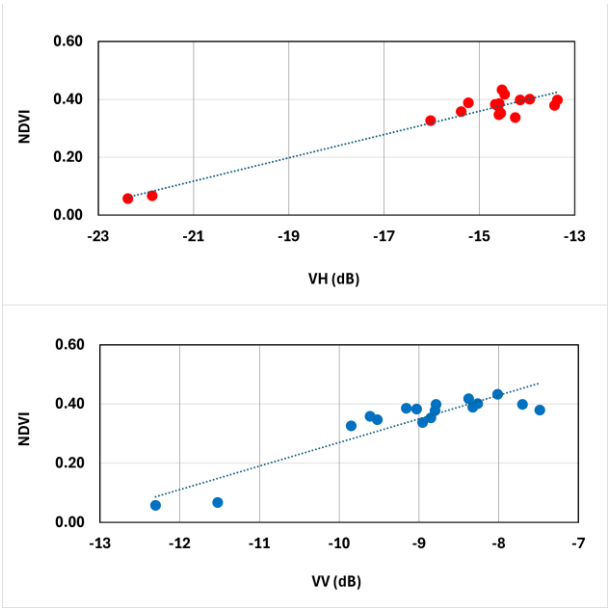

Figure 9 - Graphical representation of the relationship between σ^0_{VH} with the NDVI (red dots) and σ^0_{VV} with the NDVI (blue dots).

The Pearson correlation coefficient and R^2 were higher with σ^0_{VH}, however, σ^0_{VV} was more sensitive to small variations between plots, as can be seen between plots 4, 5, 6 and 7 (Figure 8), where

This contribution has been peer-reviewed. The double-blind peer-review was conducted on the basis of the full paper.
https://doi.org/10.5194/isprs-annals-X-3-W4-2025-85-2026 | © Author(s) 2026. CC BY 4.0 License.

σ^0_{VH} showed very similar values, while σ^0_{VV} managed to capture variations consistent with NDVI across the same plots.

Similarly, in order to perform an exploratory analysis of the variability of the SAR polarimetric indices, Figure 10 was constructed, indicating the average response of each of the 15 coffee-growing plots.

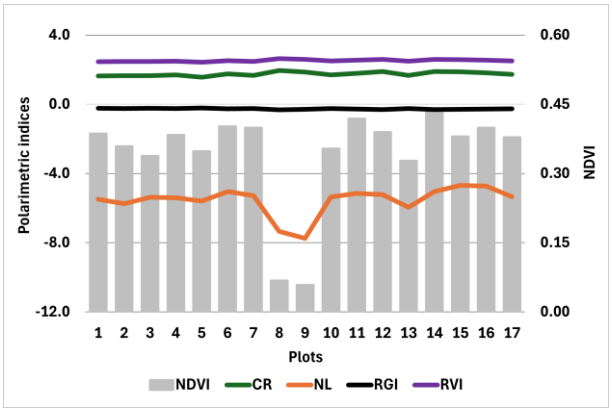

Figure 10 - Average response of the polarimetric indices CR (green line), NL (orange line), RGI (black line) and RVI (purple line) and of the NDVI of the 15 coffee plots.

Looking at Figure 10, it was possible to identify that the NL polarimetric index behaved very similarly to the NDVI, compared to the other polarimetric indices, in that their responses were basically continuous for all 15 plots.

Finally, the correlation between the NDVI optical index and each of the polarimetric indices (CR, NL, RGI, and RVI) was analyzed in order to evaluate the relationship between SAR and optical images derived from a single dataset (Figure 11).

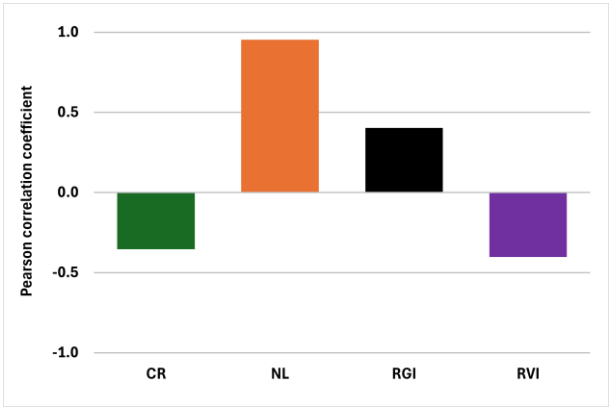

Figure 11 - Pearson correlation coefficient between the NDVI optical index and the CR, NL, RGI, and RVI polarimetric indices.

As expected, the NL polarimetric index showed the best results, with positive correlation, Pearson correlation coefficient of 0.9527, and coefficient of determination (R^2) of 0.9077. Although the other indices failed to capture the NDVI variations between plots, the RGI index showed a positive correlation, with a Pearson correlation coefficient of 0.4028 and R^2 of 0.1622. In contrast, the CR and RVI indices showed negative correlations, with Pearson correlation coefficients of -0.3543 and -0.4028, and R^2 of 0.1256 and 0.1522, respectively.

According to Mendonça et al., 2011, one of the common problems in coffee-growing regions is the spatial and temporal variability of productivity in coffee plantations, with the presence of non-productive plants alongside productive plants, as well as the biennial nature of production.

4. Conclusions

This study aimed to preliminarily explore the potential of C-SAR-Sentinel-1B images for detecting structural variations in coffee plots of different cultivars and ages in the Cerrado Mineiro. It can therefore be concluded that the temporal dynamics between the SAR backscatter coefficients and the NDVI showed a slight cyclical trend in the average backscatter values in the VH and VV polarizations, as well as in the average values of the NDVI optical index, in the 17 coffee plots. A positive correlation was found between σ^0_{VV} and NDVI in all plots, more pronounced in those that showed atypical responses. In the analysis of installments for a single date, as the average response of the NDVI vegetative index increases or decreases between the different cultivars and ages, the responses of σ^0_{VH} and σ^0_{VV} also increase or decrease, especially σ^0_{VH}, achieving a higher correlation than σ^0_{VV}. Although σ^0_{VH} achieved higher correlation, the σ^0_{VV} proved to have a better ability to capture the small variations along the coffee plots, based on NDVI. Among the polarimetric indices observed, the Normalization Ratio (NL) index was the only one that managed to capture the variations along the plots analyzed. The results obtained in this experiment show the potential of C-SAR-Sentinel-1B images for detecting structural variations in coffee plots of different cultivars and ages in the Cerrado Mineiro.

Acknowledgements

This study was financed in part by the Coordenação de Aperfeiçoamento de Pessoal de Nível Superior – Brasil (CAPES) - Finance Code 001 and Fundação de Amparo à Pesquisa do Estado de São Paulo (FAPESP) - Project 2021/06029-7. The authors extend their gratitude to Fazenda Juliana for providing the data that supported this research.

References

Abreu, K. M. P.; Coutinho, L. M. Sensoriamento remoto aplicado ao estudo da vegetação com ênfase em índice de vegetação e métricas da paisagem. Revista Vértices, v. 16, n. 2010, p. 173–198, 2014.

Arvor, D., Jonathan, M., Meirelles, M. S. P., Dubreuil, V., & Durieux, L. (2011). Classification of MODIS EVI time series for crop mapping in the state of Mato Grosso, Brazil. *International Journal of Remote Sensing*, *32*(22), 7847–7871.

Brandão, Z. N. Estimativa da produtividade e estado nutricional da cultura do algodão irrigado via técnicas de sensoriamento remoto. 2009. 152 f. Thesis (PhD in Natural Resources) - Universidade Federal de Campina Grande, Campina Grande, 2009.

Camargo, Â. P. D.; As oito fases fenológicas da frutificação do cafeeiro. In: 1998, Poços de Caldas. Anais [...]. . In: CONGRESSO BRASILEIRO DE PESQUISAS CAFEEIRAS. Poços de Caldas: Instituto Brasileiro do Café, 1998. p. 41–42.

Delécolle, R., Maas, S. J., Guerif, M., & Baret, F. Remote sensing and crop production models: present trends. *ISPRS Journal of Photogrammetry and Remote Sensing*, 47(2-3), 145- 161. 1992

ESA (European Space Agency). Sentinel Online. Available at: https://sentiwiki.copernicus.eu/web/s1-mission#S1-Mission-Satellite-Description (July 2024).

Figueiredo, D. Conceitos básicos de sensoriamento remoto. São Paulo, 2005.

Fountas, S., Espejo-García, B., Kasimati, A., Mylonas, N. e Darra, N. O futuro da agricultura digital: tecnologias e oportunidades, em IT Professional, vol. 22, não. 1, pp. 24- 28, 1 jan.-feb. 2020.

Jensen, J. R. Sensoriamento Remoto do Ambiente: Uma perspectiva em recursos terrestres. Tradução: José Carlos N. Epiphanio, et al. São José dos Campos, SP: Parêntese, 2009.

Jin, X., Kumar, L., Li, Z., Feng, H., Xu, X., Yang, G., & Wang, J. A review of data assimilation of remote sensing and crop models. *European Journal of Agronomy*, 92, 141-152. 2018.

Jönsson P, Cai Z, Melaas E, Friedl M.A., Eklundh L. A Method for Robust Estimation of Vegetation Seasonality from Landsat and Sentinel-2 Time Series Data. *Remote Sensing*. 2018; 10(4):635. https://doi.org/10.3390/rs10040635

Lee, J. A simple speckle smoothing algorithm for synthetic aperture radar images. *IEEE Transactions on Systems, Man, and Cybernetics*, n. 1, p. 85-89, 1983.

Li, Zhenwang et al. Synergetic use of DEM derivatives, Sentinel-1 and Sentinel-2 data for mapping soil properties of a sloped cropland based on a two-step ensemble learning method. *Science of The Total Environment*, p. 161421, 2023.

Mendonça, R. F.; rodrigues, W. A.; Lima, D. M.; Tomaz, M. A. Abordagem sobre a bienalidade de produção em plantas de café. [S. l.], v. 7, n. 13, p. 1–9, 2011.

Meneses, P. R.; Almeida, T. Introdução ao processamento de imagens de Sensoriamento Remoto. Universidade de Brasília – UNB. Brasília. 2012. E-book.

Moran, M. Susan et al. Ku-and C-band SAR for discriminating agricultural crop and soil conditions. *IEEE Transactions on Geoscience and Remote Sensing*, v. 36, n. 1, p. 265-272, 1998.

Paruelo, J. M.; Oesterheld, M.; Di Bella, C. M.; Arzadum, M.; Lafontaine, J.; Cahuépé, M.; Rebella, C. M. Estimation of primary production of subhumid rangelands from remote sensing data. *Applied Vegetation Science*, v. 3, p. 189–195, 2000. Available at: https://www.jstor.org/stable/1478997 (7 May 2025).

Ferreira L. T.; Cavaton, T. Produção total de café em nível mundial foi estimada em 174,9 milhões de sacas de 60kg para doze meses. [*S. l.*], 13 mar. 2025. Available at: https://www.embrapa.br/busca-de-noticias/-/noticia/99010562/artigo---producao-total-de-cafe-em-nivel-mundial-foi-estimada-em-1749-milhoes-de-sacas-de-60kg-para-doze-meses#:~:text=milh%C3%B5es%20de%20sacas.-,Dessa%20forma%2C%20constata%2Dse%20que%20o%20Brasil%2C%20maior%20produtor,%2C62%25%20da%20produ%C3%A7%C3%A3o%20global (10 June 2025).

Tolentino, F. M. Contribuição de séries temporais de atributos ópticos e SAR na discriminação do cafeeiro infestado por nematoides. Maria de Lourdes Bueno Trindade Galo. 2024. 130 f. Thesis (PhD in Cartographic Sciences) - Faculdade de Ciências e Tecnologia, Universidade Estadual Paulista, Presidente Prudente, 2023.

Ulaby, F. T.; Jedlicka, R. P. Microwave dielectric properties of plant materials. *IEEE Transactions on Geoscience and Remote Sensing*, n. 4, p. 406-415, 1984.